Post-print of: Salazar-Alvarez, German et al. “Tunable high-field magnetization in strongly exchange-coupled freestanding Co/CoO core/shell coaxial nanowires” in ***ACS applied materials & interfaces***, Vol. 8 núm 34 (Agost 2016) , p. 22477-22483. The final version is available at DOI 10.1021/acsami.6b05588

Tunable high-field magnetization in strongly exchange-coupled freestanding Co/CoO core/shell coaxial nanowires

German Salazar-Alvarez[†,*], Julian Geshev[§,‡], Sebastià Agramut-Puig[‡], Carles Navau[‡], Alvaro Sánchez[‡], Jordi Sort[‡,ǁ], Josep Nogués[Δ,ǁ,*]

[†]Department of Materials and Environmental Chemistry, Stockholm University, S-10691 Stockholm, Sweden
[§]Instituto de Física, Universidade Federal do Rio Grande do Sul, 91501-970 Porto Alegre, RS, Brazil
[‡]Departament de Física, Universitat Autònoma de Barcelona, E-08193, Bellaterra, Spain
[ǁ]ICREA, Pg. Lluís Companys 23, 08010 Barcelona, Spain
[Δ]Catalan Institute of Nanoscience and Nanotechnology (ICN2), CSIC and The Barcelona Institute of Science and Technology, Campus UAB, Bellaterra, 08193 Barcelona, Spain

ABSTRACT

The exchange bias properties of Co/CoO coaxial core/shell nanowires have been investigated with cooling and applied fields perpendicular to the wire axis. This configuration leads to unexpected exchange-bias effects. Firstly, the magnetization value at high fields is found to depend on the field-cooling conditions. This effect arises from the competition between the magnetic anisotropy and the Zeeman energies for cooling fields perpendicular to the wire axis. This allows imprinting pre-defined magnetization states to the AFM, as corroborated by micromagnetic simulations. Secondly, the system exhibits a high-field magnetic irreversibility, leading to open hysteresis loops, attributed to the AFM easy-axis reorientation during the reversal (effect similar to athermal training). A distinct way to manipulate the high-field magnetization in exchange-biased systems, beyond the archetypical effects, is thus experimentally and theoretically demonstrated.

Keywords: coaxial nanowires, exchange bias, CoO, uncopmpensated spins, training effects, high field irreversibility

1. INTRODUCTION

Partially oxidized Co(CoO) particles (with no particular anisotropic shapes) exhibit hysteresis loops shifted along the magnetic field axis after cooling in the presence of a magnetic field (i.e., exchange bias[2-4]). This is ascribed to the exchange interactions between the ferromagnetic (FM) core and the antiferromagnetic (AFM) shell. Since this effect has been technologically exploited to implement the so-called spin-valves or magnetic tunnel junctions in spintronic devices[5,6], most of the studies on exchanged biased systems have essentially focused on how to maximize this shift, as well as on how to tune the associated coercivity enhancement in thin films.[2-4,7]

It is worth mentioning that due to its large exchange coupling the Co/CoO system has been used as a reference material in exchange bias studies in thin films, lithographed structures or core/shell nanoparticle or nanowires.[1-4,7-13]

Remarkably, compared to the existing literature on exchange biased thin films[2-4] and isotropic bi-magnetic core/shell nanoparticles,[7,14] the amount of studies dealing with exchange biased anisotropic nanostructures (i.e., rods, nanowires) is relatively scarce.[15-17] Nonetheless, interesting new phenomena arising from the competition between shape anisotropy and exchange bias may be anticipated in these structures, thus providing an extra degree of freedom to enhance the current functionalities of these materials while adding large potential for novel, unforeseen, applications.

Actually, the study of one dimensional (1D) structures (e.g., nanowires, nanorods, or nanotubes), has attracted ample attention during the last few years, not only from the basic science point of view, i.e., as an intermediate case between films (2D structures) and nanoparticles (0D structures), but also for their superior properties. The interest on such type of nanostructures is actually not restricted to magnetism. Their unique performance in areas

like electronics, optics, mechanical engineering or catalysis has boosted their prospective use in diverse types of advanced and innovative nanodevices.[18–20]

Magnetic nanowires are being proposed in applications like high density magnetic recording, permanent magnets, sensors, magneto-optic devices, thermopower, microwave absorbers or in biomedicine.[18–31] More specifically, bi-magnetic coaxial nanowires are appealing for field sensors,[32] microwave absorbers,[33,34] magnetic recording[35-37] or water treatment.[38] Even though there exist some studies of bi-magnetic coaxial nanowires where the core and the shell are grown independently [thus allowing different combinations of FM, ferrimagnetic (FiM) or AFM cores and shells][17,32,34,35,37–41] the partial oxidation of FM transition metal nanowires (Fe, Co, Ni and their alloys) offers a fast and simple process to obtain bi-magnetic coaxial nanowires in a controlled manner. In this case, the core is FM and the corresponding shell is either AFM or FiM.[15-17,36,38,42–59] The exchange coupling between the FM core and the AFM or FiM shell gives rise to phenomena similar to the ones observed in thin films and nanoparticles, e.g., loop shifts and coercivity enhancement.[15-17,36,38,42–59] However, new effects could emerge if the exchange coupling is induced in such a way that it directly competes with the shape anisotropy.

So far, there have been very few systematic studies of the core/shell exchange coupling in freestanding, template-synthesized core/shell nanowires.[12,50,58,59] It is precisely this lack of in-depth studies, particularly for measuring fields applied perpendicular to the wire axis, which has so far precluded the discovery of previously not envisaged exchange bias effects in this particular geometry.

In this article we present the foremost demonstration of the possibility to manipulate the high-field magnetization states in freestanding Co/CoO core/shell nanowires, along the perpendicular-to-the-wires axis, by using exchange bias. Namely, the strong FM/AFM coupling results in striking differences between the field cooled and zero field cooled (ZFC)

loops at high fields and a high-field irreversibility at large fields in ZFC loops. This previously unreported exchange bias effect (which adds to the extensively studied loop shift and coercivity enhancement) arises from the competition between the shape/magnetocrystalline anisotropies (along the wire) and the cooling and measuring fields (perpendicular to the wire).

2. EXPERIMENTAL METHODS

2.1 Alumina anodization. Pure aluminum (99.999%) foils with a thickness of 130 μm were used as starting materials. Prior to anodization, the aluminum was annealed under air at 480 ºC for 1 h. The aluminum foils were degreased ultrasonically in acetone for 10 minutes, then etched in 240 mM Na_2CO_3 at 80 ºC for 1 min and neutralized in 36 vol% HNO_3 at 20 ºC for 20 s. Foils, 10×25 mm^2 in size, were electrochemically polished (1:5 v/v of ethanol/$HClO_4$) and then mounted as the anode with graphite as cathode in the electrochemical cell. The anodization of the aluminum pieces was carried out under 300 mM oxalic acid at 40 V at 10 ºC for 5 h. The anodic oxide cap layer was removed in a mixture of 6 wt% H_3PO_4 and 1:8 wt% chromic acid at 60 ºC for 12 h. The thus textured foil was anodized further under identical conditions to those of the first anodizing.[19,60,61] This process leads to a hexagonal array of holes with and average distance between holes of about 100±10 nm (Fig. S7).

2.2 Cobalt deposition. The cobalt was deposited by pulsed electrodeposition from an aqueous solution consisting of 4 wt% cobalt sulphate and 4 wt% boric acid, using 20 V pulses at 200 Hz at 20 ºC. A voltage reduction sequence technique was implemented to facilitate deposition of cobalt where each step lowered the voltage by 10 %. Each subsequent step was initiated once the current was recovered to a new steady state value following the previous decrement,[62] the voltage reduction sequence procedure was controlled manually to achieve 16 V.

Although potentiostatic electrodeposition might avoid problems associated with the growth of mixed phases,[63] pulse electrodeposition was employed in order to minimize variations of pH and metal ion concentration inside the pores of the alumina template during the course of electrodeposition, which would have been made the growth of the nanowires more inhomogeneous.[64-66] Pulse electrodeposition offers an additional advantage with respect to electrodeposition at a constant potential. Namely, during potentiostatic electrodeposition, hydrogen evolves continuously and could eventually block the central part of the pores, thus shielding the deposition from the pore center. Under these conditions, nanotubes (instead of nanowires) might be formed. Conversely, in pulse potential mode, the evolved hydrogen has enough time to withdraw out of the pore during the "pause time" between consecutive pulses, and the metal can fill up the whole volume of the pore, thus resulting in the growth of fully dense nanowires.

It is worth mentioning that the nanowires were not subject to an annealing treatment while still embedded in the alumina template. It is well known that the hcp-to-fcc phase transformation in Co is not fully reversible. Namely, although at high temperature, pure fcc-phase can indeed be formed, the fcc phase is usually partially retained when cooling back to room temperature (particularly in nanoparticles or nanocrystalline samples), as it often encountered in martensitic transformations.[67] It is therefore unlikely that 100% single phase hcp nanowires could be obtained by annealing. On the other hand, annealing at high temperature could cause crystallization of the anodized alumina template, which would then prevent the subsequent chemical etching to release the nanowire.[68] For these reasons, annealing treatments were not attempted in this work.

The aluminum substrate was eliminated by electrochemical etching in 20 wt% HCl solution,

with an operating voltage of 1–5 V. The alumina film was removed by dissolving it with a 2:5 M NaOH aqueous solution for 20 min at 45 ºC. The wires were washed from the reaction media by rinsing with water followed by centrifugation and finally rinsing with ethanol.

Concomitant to the dissolution of the alumina shell, exposure of the metallic cobalt nanowires to aqueous NaOH results in the formation of a (hydrated) CoO surface layer on the cobalt nanowires.[69] Note that under these conditions the CoO layer can be considered a passivation layer, thus any further oxidation of the wires in ambient conditions is not energetically favorable. Consequently, the nanowires and their magnetic properties are very stable over time.

3. RESULTS AND DISCUSSION

From the analysis of the transmission electron microscopy (TEM) images (see Supporting Information), the diameter of the wires was estimated to be D = 30±4 nm (see Figs. 1 and S1) with an average length of 5 µm, whereas the cobalt oxide shell was measured to be t_{sh} = 4±1 nm (see Figs. S1 and S2). Note that, compared to most chemically synthesized core-shell nanowires, these template-grown nanowires exhibit rather smooth surfaces with a fairly homogeneous oxide layer. This could be advantageous for certain types of applications where, for example, further functionalization or electrical contacts may be needed. Selected area electron diffraction and high resolution imaging indicate that the cobalt cores consist of hcp phase and that they exhibit a c-axis orientation roughly along the wire axis (see Fig. 1). However, the wires present some defects along the length, such as stacking faults and small regions consisting of, predominantly, fcc phase (Fig. S3); in concordance with the x-ray[70] results (see Fig. S6). The occurrence of mixed fcc and hcp phases in Co nanowires, as well as variations in crystallographic texture, have been reported by several authors depending on the electrodeposition parameters.[71,72] The electron microscopy analysis indicates that the CoO

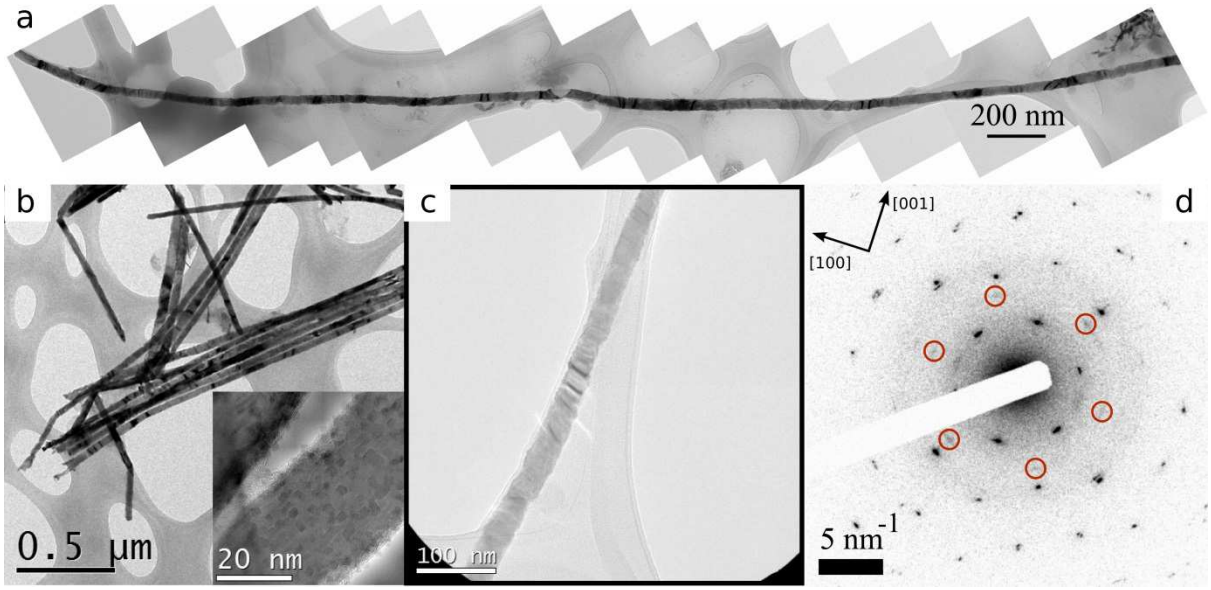

Figure 1 (**a**) Montage of low magnification TEM micrographs showing a single wire. (**b**) TEM micrograph of several nanowires where the inset shows CoO crystallites that compose the shell. (**c, d**) TEM micrograph of a single nanowire displaying stacking faults and its respective electron diffraction pattern. The arrows in the diffractogram indicate the crystallographic directions of hcp-Co phase taken from the [010] zone axis. The encircled spots correspond to the {220} interplanar distances of CoO.

shell is polycrystalline with a small crystallite size ($< D >_{CoO}$ ~ 4 nm –Fig. S4–). Quantitative analysis of the electron energy loss spectra (EELS, see Fig. S5) confirms that the shell is CoO.

The magnetic measurements (see Supporting Information) evidence that the nanowires embedded in the alumina templates exhibit properties typical for this type of wires.[19,21,23,25,73] Namely, the magnetic behavior is mainly dominated by the shape and magnetocrystalline anisotropies of Co, where the c-axis lies along the wire. Thus, when measuring along the wire, high coercivity ($\mu_0 H_C^{\parallel} \approx 150$ mT) and square-type loops are obtained (i.e., easy axis behavior), while when measuring perpendicular to the wires a sheared loop with much smaller coercivity ($\mu_0 H_C^{\perp} \approx 60$ mT) is observed, characteristic of a hard axis (see Fig. 2a).

However, the rounding of the easy-axis loop indicates that other effects, such as interactions between wires, non-perfect alignment of the c-axis with the wire axis,[63,74] or the presence of defects, e.g., stacking faults, can also play a role.[19,21,23,25] Due to the random in-plane distribution of the wires, the net effect of dipolar interactions should be practically negligible so we do not expect these to significantly affect the out-of-plane magnetic behavior of our system. Remarkably, no loop shift is observed in the embedded wires after FC, indicating the absence of any significant oxidation of the wires.[7] This is in contrast to nanowires embedded in polymeric templates which tend to slowly oxidize with time.[16,54]

The hysteresis loop of the freestanding wires at 10 K (FC and measured perpendicular to their long axis, Fig. 2b) exhibits a somewhat rounded shape (consistent with a hard-axis measurement), a remarkably large loop shift ($\mu_0 H_E \approx 120$ mT), and an enhanced coercivity ($\mu_0 H_C \approx 120$ mT) compared to the hard axis measurements of the nanowires inside the template. These properties arise from the presence of a FM-AFM coupling between the FM Co core and the AFM CoO shell[7]. Similarly, the presence of a strong asymmetry between the increasing and decreasing field branches of the loop (see top inset in Fig. 2b) is also a distinctive signature of exchange bias.[2-4,7] Interestingly, the interface exchange energy (taking into account the cylindrical symmetry[7]), $\Delta E = 0.94$ erg/cm^2, is considerably large.[2] These values are much greater than most literature ones for coaxial Co/CoO wires [except Co/CoO nanotubes, with $\Delta E = 1.14$ erg/cm^2 (ref. 58,59)] and in concordance with high quality Co-CoO thin films, Co nanoparticles embedded in CoO or NiO matrices, lithographed nanostructures or Co-CoO core-shell nanoparticles.[9,10,12,75,76]

Notably, in thin films it has been shown that no exchange bias can be induced when they are FC perpendicular to the either FM or AFM easy axes.[77,78] In contrast, in systematic studies of lithographically patterned FM-AFM lines it has been demonstrated that although the exchange bias depends strongly on the cooling-field direction, loop shifts are induced even

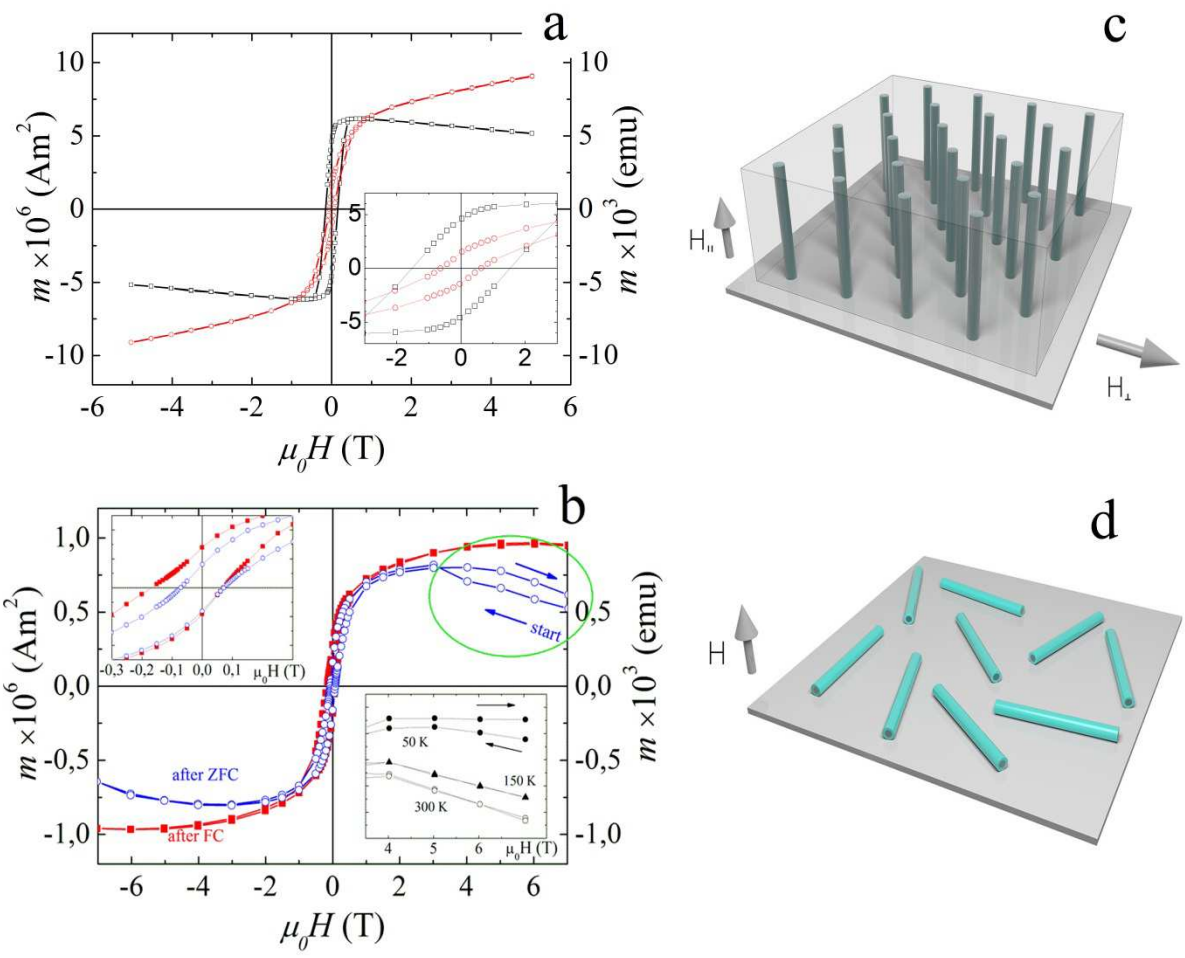

Figure 2. (**a**) Hysteresis loops of the aligned cobalt wires embedded in the anodised alumina membrane measured at 10 K (after field cooling) parallel (–□–) and perpendicular (–○–) to the nanowire axis, respectively. (**b**) Out-of-plane hysteresis loops for free-standing of Co|CoO core-shell nanowires traced at 10 K starting from +7 T after either ZFC (–○–) or FC in 5 T (–■–) from 300 K. The top inset shows a magnification of the low field region of the loops. The bottom inset shows the high field magnetization measured at 50, 150 and 300 K, after ZFC. No diamagnetic correction has been performed to any of the loops. The lines are guides to the eye. The ellipse in (b) highlights the high-field irreversibility. Panels (**c**) and (**d**) show schematically the direction of the measuring field and the arrangement of the wires for the ones embedded in the alumina template and for the free-standing ones deposited on a Colodion membrane, respectively.

when cooling perpendicular to the wire axis,[79-81] in agreement with our results in coaxial Co-CoO nanowires. In fact, coherent rotation models predict the existence of H_E even though with $H_C = 0$ (Refs. 79,80). The fact that the Co-CoO nanowires exhibit a moderately large H_C implies that the reversal occurs probably not through coherent rotation but by more complex reversal modes as reported in non-oxidized wires of different sizes.[19,21,23,25,73]

As can be seen in Fig. 2b, the FC and FZC loops of the free-standing wires show strikingly different behaviors at high fields. The large difference in the high-field magnetization between the FC and ZFC curves can be attributed to the effect of the imprinted magnetic states in the AFM shell by the FM core during the cooling procedure (see Figs. 3 a-d).[77,82] At low temperatures, the strong exchange coupling between the imprinted AFM magnetic states and the FM magnetization controls the magnetization process. At room temperature, the AFM part of the wires is paramagnetic; thus, it does not contribute to the magnetization orientation of the core. At this temperature the direction of the Co moments is dictated mainly by the magnetocrystalline and shape anisotropies, both aligned along the nanowire length. Consequently, at zero field most of the Co moments lie along the wire (perpendicular to the measuring field). However, the presence of stacking faults and fcc inclusions results in some local misalignment of the magnetization (see Fig. 3a). The ZFC process, starting from 300 K, does not change the direction of the FM magnetic moments from their local easy axes. This implies that during the cooling process the local FM magnetization directions are imprinted into the AFM shell (Fig. 3a). At low temperature, since the FM and AFM spins are strongly coupled at the interface (as evidenced from the large value of H_E), the FM moments prefer to remain in the vicinities of their local easy-axis directions pinned by the imprinted domains in the AFM. Hence, +7 T magnetic field is far from being sufficiently high to align all of the FM moments along the out-of-plane direction (Fig. 3c). This leads to a small high-field FM signal. In contrast, when a strong field is applied at room temperature, the FM magnetization

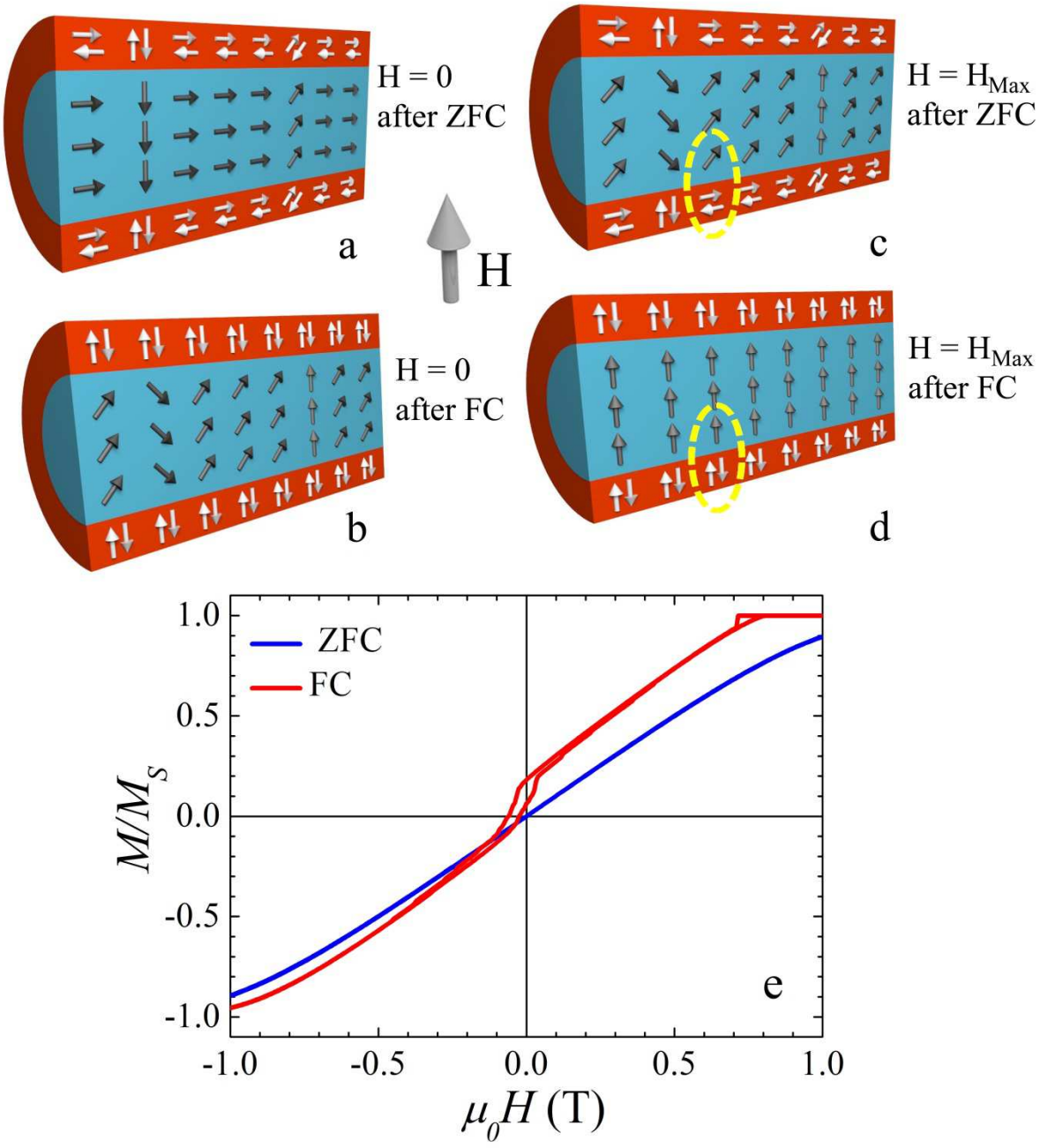

Figure 3. Schematic representation of the AFM and FM spin structure at H = 0 after (**a**) ZFC and (**b**) FC perpendicular to the wire and at H_{Max} (where H_{Max} is the maximum measuring field) after (**c**) ZFC and (**d**) FC perpendicular to the wire. (**e**) Simulated low temperature hysteresis loops after FC and ZFC treatments. Highlighted by dashed ellipses in (c) and (d) is the behavior of some representative spins in the core and the shell for the two cooling procedures.

is nearly saturated perpendicular to the wire axis. Thus, during the FC procedure the perpendicular magnetization information is imprinted in the AFM (Fig. 3). Accordingly, due to the interface coupling at low temperatures the FM magnetizations prefer to be aligned along the imprinted AFM domains (perpendicular to the wire axis) and the high-field magnetization value is large.

To corroborate this picture we have performed some micromagnetic simulations using an "uncompensated spins" model[83] (see Supporting Information). As can be seen in Fig. 3e, as expected, the simulated ZFC hysteresis loop shows no bias and a vanishing H_C as opposed to the FC one. Importantly, the magnetization of the ZFC wire is more difficult to saturate than the field-cooled one. This implies that for moderately large fields the magnetization of the ZFC loop is smaller than that of the FC one, in qualitative agreement with the experimental results (despite the simplicity of the model).

Note that the concept of competing anisotropies is well established in both exchange biased thin films and lithographed FM/AFM structures.[79-81,84-87] However, the anisotropies involved in these systems are usually much smaller than for Co/CoO nanowires, thus, the high-field differences between FC and ZFC loops were not previously observed.

Another unreported outstanding feature of the Co/CoO wires is the high-field irreversibility observed at positive fields. Namely, at high fields (far above the anisotropy field, i.e., where the loop closes) the loop does not retrace itself (see highlighting ellipse in Fig. 2b). Notably, as the temperature is increased the effect becomes weaker, disappearing at about 150 K (see inset of Fig. 2b). This unusual effect is, most probably, due to the field-induced reorientation of the imprinted AFM magnetic information, which leads to a realignment of the FM magnetization. That is, at low temperature and after ZFC, each of the imprinted AFM moments is oriented along its easy axis closest to the direction of the local FC magnetization. During the loop trace, some of the AFM moments are dragged by the FM ones. Since CoO

has a cubic magnetocrystalline anisotropy (with more than one easy axis), after the magnetization reversal some of the AFM moments may have found a more stable direction (i.e., they settle in the vicinity a new, equivalent, easy axis). This process would be alike the exchange-bias athermal training[88,89] effect proposed by Hoffmann,[90] which, as it has been shown, may even lead to a positive exchange bias.[91] Due to this AFM reorientation and the strong AFM/FM coupling, the FM realigns slightly trying to line up along the new local AFM direction, leading to the observed irreversibility. Importantly, retracing the loop at 10 K results in a virtually closed high-field part of the loop, a result expected from a training-like effect. Subsequent loops show no change at high fields. Similarly, H_E slightly decreases from the first to the second loop, remaining nearly constant for higher number of loops. Given that as the temperature is increased the AFM anisotropy decreases, the strength of the coupling reduces and the AFM is progressively less effective in reorienting the FM.

4. CONCLUSIONS

To summarize, we have demonstrated two new exchange bias effects in core/shell, coaxial Co/CoO freestanding nanowires: (i) dependence of the high-field magnetization on the cooling procedure and (ii) high-field irreversibility in the ZFC loops. Both novel properties are observed in measurements acquired perpendicular to the wire axis. This geometry leads to a competition between the intrinsic anisotropies of the Co core (shape and magnetocrystalline – along the wire axis), the applied field, and the magnetic states imprinted in the CoO shell by the cooling procedures. Micromagnetic simulations qualitatively confirm the critical role played by the AFM in achieving the difference between the ZFC and FC high field magnetizations. The tunability of the high-field magnetization by the exchange coupling provides an additional degree of freedom for the design of spintronic devices.

ASSOCIATED CONTENT

Supporting Information

The Supporting Information is available free of charge on the ACS Publications website at DOI:

Additional characterization (TEM, XRD and SEM) and micromagnetic simulations.

AUTHOR INFORMATION

Corresponding Authors

***E-mail:** german@mmk.su.se (G.S.A.)

***E-mail:** josep.nogues@uab.cat (J.N.)

Notes

The authors declare no competing financial interest.

ACKNOWLEDGEMENTS

The work was supported by the 2014-SGR-1015 and 2014-SGR-150 projects of the Generalitat de Catalunya, the Spanish MAT2012-35370 project, European Community's Seventh Framework Programme (FET-Open/FP7/2007-2013) under grant agreement 296679 (MANAQA) and the Brazilian agency CAPES (BEX 0298/2015-08). GSA thanks the Knut and Alice Wallenberg Foundation (Project 3DEM-NATUR) for the partial financial support. AS acknowledges the funding from an ICREA Academia award. The authors thank María Esther Mata-Zamora and Raul Valenzuela for providing the nanowires. ICN2 acknowledges support from the Severo Ochoa Program (MINECO, Grant SEV-2013-0295).

REFERENCES

(1) Meiklejohn, W. H.; Bean, C. P. New Magnetic Anisotropy. *Phys. Rev.* **1956**, *102*, 1413-1415.

(2) Nogués, J.; Schuller, I. K. Exchange Bias. *J. Magn. Magn. Mater*. **1999**, *192*, 203-232.

(3) Shi, Z.; Du J.; Zhou, S.-M. Exchange Bias in Ferromagnet/Antiferromagnet Bilayers. *Chin. Phys. B* **2014**, *23*, 027503.

(4) Dieny, B.; Speriosu, V. S.; Parkin, S. S. P.; Gurney, B. A.; Wilhoit D. R.; Mauri, *D.* Giant Magnetoresistance in Soft Ferromagnetic Multilayers. *Phys. Rev. B: Condens. Matter*, **1991**, *43*, 1297-1300.

(5) Parkin, S.; Xin, J.; Kaiser, C.; Panchula, A.; Roche, K.; Samant, A. Magnetically Engineered Spintronic Sensors and Memory. *Proc. IEEE* **2003**, *91*, 661-680.

(6) Nogués, J.; Sort, J.; Langlais, V.; Skumryev, V.; Suriñach, S.; Muñoz, J. S.; Baró, M. D. Exchange Bias in Nanostructures. *Phys. Rep.* **2005**, *422*, 65-117.

(7) Miltényi, P.; Gierlings, M; Keller, J.; Beschoten, B.; Güntherodt, G.; Nowak, U.; Usadel, K. D. Diluted Antiferromagnets in Exchange Bias: Proof of the Domain State Model. *Phys. Rev. Lett.* **2000**, *84*, 4224-4227.

(8) Gredig, T.; Krivorotov, I. N.; Dahlberg, E. D. Temperature Dependence of Magnetization Reversal and Angular Torque in Co/CoO. *Phys. Rev. B: Condens. Matter* **2006**, *74*, 094431.

(9) Laureti, S.; Suck, S. Y.; Haas, H.; Prestat, E.; Bourgeois, O.; Givord, D. Size Dependence of Exchange Bias in Co/CoO Nanostructures. *Phys. Rev. Lett.* **2011**, *108*, 077205.

(10) Feygenson, M.; Yiu, Y.; Kou, A.; Kim, K.-S.; Aronson, M. C. Controlling the Exchange Bias Field in Co Core/CoO Shell Nanoparticles. *Phys. Rev. B: Condens. Matter* **2010**, *81*, 195445.

(11) Maurer, T; Zighem, F.; Ott, F.; Chaboussant, G.; André, G.; Soumare, Y.; Piquemal, J.- Y.; Viau, G.; Gatel, C. Exchange Bias in Co/CoO Core-Shell Nanowires: Role of Antiferromagnetic Superparamagnetic Fluctuations. *Phys. Rev. B: Condens. Matter* **2009**, *80*, 064427.

(12) López-Ortega, A.; Estarder, M.; Salazar-Alvarez, G.; Roca, A.G.; Nogués, J. Applications of Exchange Coupled Bi-Magnetic Hard/Soft and Soft/Hard Magnetic Core/Shell Nanoparticles. *Phys. Rep*. **2015**, *553*, 1-32.

(13) Maaz, K.; Kim, S. H.; Jung M.- H.; Kim, G.- H. Effect of Temperature on the Exchange Bias in Naturally Oxidized Ni_xCo_{1-x} (x = 0.2) Nanowires Fabricated by Electrochemical Deposition Technique. *J. Alloys Compd*. **2012**, *520*, 272-276.

(14) Medina, J. D. L. T.; Darques, M.; Piraux, L. Exchange Bias Anisotropy in Co Nanowires Electrodeposited into Polycarbonate Membranes. *J. Appl. Phys*. **2009**, *106*, 023921.

(15) Kazakova, O.; Daly, B.; Holmes, J. D. Tunable Magnetic Properties of Metal/Metal Oxide Nanoscale Coaxial Cables. *Phys. Rev. B: Condens. Matter* **2006**, *74*, 184413.

(16) Xu, X.; Fang, X.; Zeng, H.; Zhai, T.; Bando Y.; Golberg, D. One-Dimensional Nanostructures in Porous Anodic Alumina Membranes. *Sci. Adv. Mater*. **2010**, *2*, 273-294.

(17) Sousa, C. T.; Leitao, D. C.; Proenca, M. P.; Ventura, J.; Pereira, A. M.; Araujo, J. P. Nanoporous Alumina as Templates for Multifunctional Applications. *Appl. Phys. Rev*. **2014**, *1*, 031102.

(18) Clime, L.; Drogoff, B. L.; Zhao, S.; Zhang, Z.; Veres, T. Magnetic Nanocarriers: from Material Design to Magnetic Manipulation. *Int. J. Nanotechnol.* **2008**, *5*, 1268-1305.

(19) Valenzuela, R.; Alvarez, G.; Mata-Zamora, M. E. Microwave Properties of Ferromagnetic Nanostructures. *J. Nanosci. Nanotechnol*. **2008**, *8*, 2827-2835.

(20) Tian, Y.; Bakaul, S. R.; Wu, T. Oxide Nanowires for Spintronics: Materials and Devices. *Nanoscale* **2012**, *4*, 1529-1540.

(21) Kou, X.; Fan, X.; Dumas, R. K.; Lu, Q.; Zhang, Y.; Zhu, H.; Zhang, X.; Liu, K.; Xiao, J. Q. Memory Effect in Magnetic Nanowire Arrays. *Adv. Mater*. **2011**, *23*, 1393-1397.

(22) Liakakos, N.; Blon, T.; Achkar, C.; Vilar, V.; Cormary, B.; Tan, R. P.; Benamara, O.; Chaboussant, G.; Ott, F.; Warot-Fonrose, B.; Snoeck, E.; Chaudret, B.; Soulantica, K.; Respaud, M. Solution Epitaxial Growth of Cobalt Nanowires on Crystalline Substrates for Data Storage Densities beyond 1 Tbit/in^2. *Nano Lett*. **2014**, *14*, 3481-3486.

(23) González-Díaz, J. B.; García-Martín, A.; Armelles, G.; Navas, D.; Vázquez, M.; Nielsch, K.; Wehrspohn, R. B.; Gösele, U. Enhanced Magneto-Optics and Size Effects in Ferromagnetic Nanowire Arrays. *Adv. Mater*. **2007**, *19*, 2643-2647.

(24) Hultgren, A.; Tanase, M.; Felton, E. J.; Bhadriraju, K.; Salem, A. K.; Chen, C. S.; Reich, D. H. Optimization of Yield in Magnetic Cell Separations Using Nickel Nanowires of Different Lengths. *Biotechnol. Prog*. **2005**, *21*, 509-515.

(25) Böhnert, T.; Vega, V.; Michel, A.-K.; Prida, V.M.; Nielsch, K. Magneto-Thermopower and Magnetoresistance of Single Co-Ni Alloy Nanowires. *Appl. Phys. Lett.* **2013**, *103*, 092407.

(26) Chan, K.; Doran, C.; Shipton, E.; Fullerton, E. E. Core-Shell Structured Nanowire Spin Valves. *IEEE Trans. Magn*. **2010**, *46*, 2209-2211.

(27) Chiscan, O.; Dumitru, I.; Tura, V.; Chiriac, H.; Stancu, A. High Frequency Absorption of PVC/Iron Oxides and PVC/$CoFe_2O_4$/CoO Nanofibers Produced by Electrospinning Technique. *IEEE Trans. Magn*. **2011**, *47*, 4511-4516.

(28) Chong, Y. T.; Görlitz, D.; Martens, S.; Yau, E. M. Y.; Allende, S.; Bachmann, J.; Nielsch, K. Multilayered Core/Shell Nanowires Displaying Two Distinct Magnetic Switching Events. *Adv. Mater*. **2010**, *22*, 2435-2439.

(29) Ivanov, Y. P.; Chuvilin, A.; Lopatin, S.; Kosel, J. Modulated Magnetic Nanowires for Controlling Domain Wall Motion: Toward 3D Magnetic Memories. *ACS Nano* **2016**, *10*, 5326–5332.

(30) Ai, Z.; Wang, Y.; Xiao, M.; Zhang, L.; Qiu, J. Microwave-Induced Catalytic Oxidation of RhB by a Nanocomposite of Fe@Fe_2O_3 Core/Shell Nanowires and Carbon Nanotubes. *J. Phys. Chem. C* 2008, **112**, 9847-9853.

(31) Daly, B.; Arnold, D. C.; Kulkarni, J. S.; Kazakova, O.; Shaw, M. T.; Nikitenko, S.; Erts, D.; Morris, M. A.; Holmes, J. D. Synthesis and Characterization of Highly Ordered Cobalt–Magnetite Nanocable Arrays. *Small* **2006**, *2*, 1299-1307.

(32) Chen, J. Y.; Ahmad, N.; Shi, D. W.; Zhou, W. P.; Han, X. F. Synthesis and Magnetic Characterization of Co-NiO-Ni Core-Shell nanotube arrays. *J. Appl. Phys*. **2011**, *110*, 073912.

(33) Sudakar, C.; Subbanna, G.; Kutty, T. Nanoparticle Composites Having Structural Intergrowths of Hexaferrite and Spinel Ferrites Prepared by Gel-to-Crystallite Conversion and their Magnetic Properties. *J. Magn. Magn. Mater*. **2004**, *268*, 75-88.

(34) Lo, C.- C.; Huang, C.- C. ; Liu, C.- M.; Chen, C.; Kuo, C.- Y.; Lin, H.- J.; Tseng, Y.- C. Magnetic Properties of Electroless-Deposited Ni and Ni–NiO Core–Shell Nano-Arrays. *J. Magn. Magn. Mater*. **2011**, *323*, 1950-1953.

(35) Lee, J. H.; Wu, J. H.; Lee, J. S.; Jeon, K. S.; Kim, H. R.; Lee, J. H.; Suh, Y. D.; Kim, Y. K. Synthesis and Characterization of Fe-FeO_x Core-Shell Nanowires. *IEEE Trans. Magn*. **2008**, *44*, 3950-3953.

(36) Chen, Y. J.; Gao, P.; Zhu, C. L.; Wang, R. X.; Wang, L. J.; Cao, M. S.; Fang, X. Y. Synthesis, Magnetic and Electromagnetic Wave Absorption Properties of Porous Fe_3O_4/Fe/SiO_2 Core/Shell Nanorods. *J. Appl. Phys*. **2009**, *106*, 054303.

(37) Yang, J. B.; Xu, H.; You, S. X.; Zhou, X. D.; Wang, C. S.; Yelon, W. B.; James, W. J. Large Scale Growth and Magnetic Properties of Fe and Fe_3O_4 Nanowires. *J. Appl. Phys.* **2006**, *99*, 08Q507.

(38) Lu, L.; Ai, Z.; Li, J.; Zheng, Z.; Li, Q.; Zhang, L. Synthesis and Characterization of Fe/Fe_2O_3 Core/Shell Nanowires and Nanonecklaces. *Cryst. Growth Des.* **2007**, *7*, 459-464.

(39) Grzelczak, M.; Correa-Duarte, M. A.; Salgueiriño-Maceira, V.; Rodríguez-González, B.; Rivas, J.; Liz-Marzán, L. M. Pt-Catalyzed Formation of Ni Nanoshells on Carbon Nanotubes. *Angew. Chem. Int. Ed*. **2007**, *46*, 7026-7030.

(40) Salgueiriño-Maceira, V.; Correa-Duarte, M. A.; Bañobre-López, M.; Grzelczak, M.; Farle, M.; Liz-Marzán, L. M.; Rivas, J. Magnetic Properties of Ni/NiO Nanowires Deposited onto CNT/Pt Nanocomposites. *Adv. Funct. Mater*. **2008**, *18*, 616-621.

(41) Hsu, H.-C.; Lo, C.-C.; Tseng, Y.-C. Competing Magnetic Interactions and Interfacial Frozen Spins in Ni-NiO Core-Shell Nano-Rods. *J. Appl. Phys*. **2012**, *111*, 063919.

(42) Pan, H.; Yi, J.; Liu, B.; Thongmee, S.; Ding, J.; Feng, Y. P.; Lin, J. Y. Magnetic Properties of Highly-Ordered Ni, Co and Their Alloy Nanowires in AAO Templates. *Solid State Phenom.* **2006**, *111*, 123-126.

(43) Vila, L.; George, J. M.; Faini, G.; Popa, A.; Ebels, U.; Ounadjela, K.; Piraux, L. Transport and Magnetic Properties of Isolated Cobalt Nanowires. *IEEE Trans. Magn.* **2002**, *38*, 2577-2579.

(44) Ursache, A.; Goldbach, J. T.; Russell, T. P.; Tuominen, M. T. Pulse Electrodeposition and Electrochemical Quartz Crystal Microbalance Techniques for High Perpendicular Magnetic Anisotropy Cobalt Nanowire Arrays. *J. Appl. Phys*. **2005**, *97*, 10J322.

(45) Maaz, K.; Ishrat, S.; Karim, S.; Kim, G.-H. Effect of Aging on the Magnetic Characteristics of Nickel Nanowires Embedded in Polycarbonate. *J. Appl. Phys*. **2011**, *110*, 013908.

(46) Kim, S. I.; Yoon, H.; Lee, H.; Lee, S.; Jo, Y.; Lee, S.; Choo, J.; Kim, B. Epitaxy-Driven Vertical Growth of Single-Crystalline Cobalt Nanowire Arrays by Chemical Vapor Deposition. *J. Mater. Chem. C* **2015**, *3*, 100-106.

(47) Liébana-Viñas, S.; Wiedwald, U.; Elsukova, A.; Perl, J.; Zingsem, B.; Semisalova, A. S.; Salgueiriño, V.; Spasova, M.; Farle, M. Structure-Correlated Exchange Anisotropy in Oxidized $Co_{80}N_{i20}$ Nanorods. *Chem. Mater.* **2015**, *27*, 4015–4022.

(48) Proenca, M. P.; Ventura, J.; Sousa, C. T.; Vazquez, M.; Araujo J. P. Exchange Bias, Training Effect, and Bimodal Distribution of Blocking Temperatures in Electrodeposited Core-Shell Nanotubes. *Phys. Rev. B: Condens. Matter* **2013**, *87*, 134404.

(49) Masuda, M.; Fukuda, K. Ordered Metal Nanohole Arrays Made by a Two-Step Replication of Honeycomb Structures of Anodic Alumina. *Science* **1995**, *268*, 1466-1468.

(50) Shawaqfeh, A. T.; Baltus, R. E. Fabrication and Characterization of Single Layer and Multi-Layer Anodic Alumina Membranes. *J. Membr. Sci*. **1999**, *157*, 147-158.

(51) Pirota, K. R.; Béron, F.; Zanchet, D.; Rocha, T. C. R.; Navas, D.; Torrejón, J.; Vazquez, M.; Knobel, M. Magnetic and Structural Properties of fcc/hcp Bi-Crystalline Multilayer Co Nanowire Arrays Prepared by Controlled Electroplating. *J. Appl. Phys.* **2011**, *109*, 083919.

(52) Darques, M.; Piraux, L.; Encinas, A.; Bayle-Guillemaud, P.; Popa, A.; Ebels, U. Electrochemical Control and Selection of the Structural and Magnetic Properties of Cobalt Nanowires. *Appl. Phys. Lett.* **2005**, *86*, 072508.

(53) Tsyntsaru, N.; Silkin, S.; Cesiulis, H.; Guerrero, M.; Pellicer, E.; Sort, J. Toward Uniform Electrodeposition of Magnetic Co-W Mesowires Arrays: Direct Versus Pulse Current Deposition. *Electrochim. Acta* **2016**, *188*, 589–601.

(54) Tolédano, P.; Krexner, G.; Prem, M.; Weber, H.-P.; Dmitriev, V. P. Theory of the Martensitic Transformation in Cobalt. *Phys. Rev. B: Condens. Matter* **2001**, *64*, 144104.

(55) Lindo, A. M.; Pellicer, E.; Zeeshan, M. A.; Grisch, R.; Qiu, F.; Sort, J.; Sakar, M. S.; Nelson, B. J.; Pané, S. The Biocompatibility and Anti-Biofouling Properties of Magnetic Core–Multishell Fe@C NWs–AAO Nanocomposites. *Phys. Chem. Chem. Phys.* **2015**, *17*, 13274–13279.

(56) Sato, N. Anodic Oxidation of Cobalt in Neutral and Basic Solution. *J. Electrochem. Soc*. **1978**, *125***,** 1735-1740.

(57) Jang, B.; Pellicer,E.; Guerrero, M.; Chen, X.; Choi, H.; Nelson, B. J.; Sort, J.; Pané, S. Fabrication of Segmented Au/Co/Au Nanowires: Insights in the Quality of Co/Au Junctions. *ACS Appl. Mater. & Interf.* **2014**, *6*, 14583-14589.

(58) Qin, J.; Nogués, J.; Mikhaylova, M.; Roig, A.; Muñoz, J. S.; Muhammed, M. Differences in the Magnetic Properties of Co, Fe, and Ni 250-300 nm Wide Nanowires Electrodeposited in Amorphous Anodized Alumina Templates. *Chem. Mater*. ***2005****, 17*, 1829-1834.

(59) De Toro, J. A.; Marques, D. P.; Muñiz, P.; Skumryev, V.; Sort, J.; Givord, D.; Nogués, J. High Temperature Magnetic Stabilization of Cobalt Nanoparticles by an Antiferromagnetic Proximity Effect. *Phys. Rev. Lett.* **2015**, *115*, 057201.

(60) Nogués, J.; Stepanow, S.; Bollero, A.; Sort, J.; Dieny, B.; Nolting, F.; Gambardella, P. Simultaneous in-Plane and Out-of-Plane Exchange Bias Using a Single Antiferromagnetic Layer Resolved by X-Ray Magnetic Circular Dichroism. *Appl. Phys. Lett.* **2009**, *95*, 152515.

(61) Nogués, J.; Moran, T. J.; Lederman, D.; Schuller, I. K.; Rao, K. V. Role of Interfacial Structure on Exchange-Biased FeF_2/Fe. *Phys. Rev. B: Condens. Matter*, **1999**, *59*, 6984-6993.

(62) Hoffmann, A.; Grimsditch, M.; Pearson, J. E.; Nogués, J.; Macedo, W. A .A.; Schuller, I. K. Tailoring the Exchange Bias Via Shape Anisotropy in Ferromagnetic/Antiferromagnetic Exchange-Coupled Systems. *Phys. Rev. B: Condens. Matter* **2003**, *67*, 220406.

(63) Chung, S. H.; Hoffmann, A.; Grimsditch, M. Interplay between Exchange Bias and Uniaxial Anisotropy in a Ferromagnetic/Antiferromagnetic Exchange-Ccoupled system. *Phys. Rev. B: Condens. Matter* **2005**, *71*, 214430.

(64) Tripathy, D.; Adeyeye, A. O.; Chakrabarti. K.; Singh, N. Tuning the Exchange Bias in Large Area Co/CoO Nanowire Arrays. *J. Appl. Phys*. **2010**, *107*, 09D705.

(65) Salazar-Alvarez, G.; Kavich, J. J.; Sort, J.; Mugarza, A.; Stepanow, S.; Potenza, A.; Marchetto, H.; Dhesi, S.S.; Baltz, V.; Dieny, B.; Weber, A.; Heyderman, L. J.; Nogués, J.; Gambardella, P. Direct Evidence of Imprinted Vortex States in the Antiferromagnet of Exchange Biased Microdisks. *Appl. Phys. Lett*. **2009**, *95*, 012510.

(66) Gilbert, D. A.; Ye, L.; Varea, A.; Agramunt-Puig, S.; del Valle, N.; Navau, C.; López-Barbera, J. F.; Buchanan, K.S.; Hoffmann, A.; Sánchez, A.; Sort, J.; Liu, K.; Nogués, J. Novel Reversal Mode in Exchange Coupled Antiferromagnetic/Ferromagnetic Disks. *Nanoscale* **2015**, *7*, 9878-9885.

(67) Zhang, W.; Bowden, M. E.; Krishnan, K. M. Competing Effects of Magnetocrystalline Anisotropy and Exchange Bias in Epitaxial Fe/IrMn Bilayers. *Appl. Phys. Lett*. **2011**, *98*, 092503

(68) Jiménez, E.; Camarero, J.; Sort, J.; Nogués, J.; Mikuszeit, N.; García-Martín, J. M.; Hoffmann, A.; Dieny, B.; Miranda, R. Emergence of Noncollinear Anisotropies from Interfacial Magnetic Frustration in Exchange-Bias Systems. *Phys. Rev. B: Condens. Matter* **2009**, *80*, 014415

(69) Zhang, W.; Weiss, D. N.; Krishnan, K. M. Competing Anisotropies and Temperature Dependence of Exchange Bias in Co-IrMn Metallic Wire Arrays Fabricated by Nanoimprint Lithography. *J. Appl. Phys*. **2010**, *107*, 09D724.

(70) Menendez, E.; Demeter, J.; Van Eyken, J.; Nawrocki, P.; Jedryka, E.; Wojcik, M.; López-Barbera, J. F.; Nogués, J.; Vantomme, A.; Temst, K. Improving the Magnetic Properties of Co−CoO Systems by Designed Oxygen Implantation Profiles. *ACS Appl. Mater. Interfaces* **2013**, *5*, 4320 −4327.

(71) Hoffmann, A. Symmetry Driven Irreversibilities at Ferromagnetic-Antiferromagnetic Interfaces. *Phys. Rev. Lett.* **2004**, 93, 097203.

(72) Harres, A.; Geshev, J. Athermal Training Due to Exchange Bias and Dipolar Coupling Within a Granular Model for Exchange Bias. *J. Phys.: Condens. Matter* **2011**, *23*, 216003.

Table of Content Graphic